frontiers | Frontiers in Materials

TYPE Original Research
PUBLISHED 24 February 2023
DOI 10.3389/fmats.2023.1114665

OPEN ACCESS

EDITED BY
Noor Saeed Khan,
University of Education Lahore, Pakistan

REVIEWED BY
Ghulam Rasool,
Beijing University of Technology, China
Kanayo Kenneth Asogwa,
Nigeria Maritime University, Nigeria

*CORRESPONDENCE
Sayed M. Eldin,
sayed.eldin22@fue.edu.eg

SPECIALTY SECTION
This article was submitted to Colloidal Materials and Interfaces, a section of the journal Frontiers in Materials

RECEIVED 02 December 2022
ACCEPTED 07 February 2023
PUBLISHED 24 February 2023

CITATION
Ali Q, Amir M, Raza A, Khan U, Eldin SM, Alotaibi AM, Elattar S and Abed AM (2023), Thermal investigation into the Oldroyd-B hybrid nanofluid with the slip and Newtonian heating effect: Atangana–Baleanu fractional simulation. *Front. Mater.* 10:1114665.
doi: 10.3389/fmats.2023.1114665

Thermal investigation into the Oldroyd-B hybrid nanofluid with the slip and Newtonian heating effect: Atangana–Baleanu fractional simulation

Qasim Ali[1], Muhammad Amir[1], Ali Raza[1,2], Umair Khan[3,4], Sayed M. Eldin[5]*, Abeer M. Alotaibi[6], Samia Elattar[7] and Ahmed M. Abed[8,9]

[1]Department of Mathematics, University of Engineering and Technology, Lahore, Pakistan, [2]School of Mathematics, Minhaj University, Lahore, Pakistan, [3]Department of Mathematical Sciences, Faculty of Science and Technology, Universiti Kebangsaan Malaysia, Selangor, Malaysia, [4]Department of Mathematics and Social Sciences, Sukkur IBA University, Sukkur, Sindh, Pakistan, [5]Center of Research, Faculty of Engineering, Future University in Egypt, New Cairo, Egypt, [6]Department of Mathematics, Faculty of Science, University of Tabuk, Tabuk, Saudi Arabia, [7]Department of Industrial & Systems Engineering, College of Engineering, Princess Nourah bint Abdulrahman University, Riyadh, Saudi Arabia, [8]Department of Industrial Engineering, College of Engineering, Prince Sattam Bin Abdulaziz University, Alkharj, Saudi Arabia, [9]Industrial Engineering Department, Faculty of Engineering, Zagazig University, Zagazig, Egypt

The significance of thermal conductivity, convection, and heat transportation of hybrid nanofluids (HNFs) based on different nanoparticles has enhanced an integral part in numerous industrial and natural processes. In this article, a fractionalized Oldroyd-B HNF along with other significant effects, such as Newtonian heating, constant concentration, and the wall slip condition on temperature close to an infinitely vertical flat plate, is examined. Aluminum oxide (Al_2O_3) and ferro-ferric oxide (Fe_3O_4) are the supposed nanoparticles, and water (H_2O) and sodium alginate ($C_6H_9NaO_7$) serve as the base fluids. For generalized memory effects, an innovative fractional model is developed based on the recently proposed Atangana–Baleanu time-fractional (AB) derivative through generalized Fourier and Fick's law. This Laplace transform technique is used to solve the fractional governing equations of dimensionless temperature, velocity, and concentration profiles. The physical effects of diverse flow parameters are discussed and exhibited graphically by Mathcad software. We have considered $0.15 \le \alpha \le 0.85, 2 \le Pr \le 9, 5 \le Gr \le 20, 0.2 \le \phi_1, \phi_2 \le 0.8, 3.5 \le Gm \le 8,\ 0.1 \le\ Sc\ \le 0.8$, and $0.3 \le \lambda_1, \lambda_2 \le 1.7$. Moreover, for validation of our present results, some limiting models, such as classical Maxwell and Newtonian fluid models, are recovered from the fractional Oldroyd-B fluid model. Furthermore, comparing the results between Oldroyd-B, Maxwell, and viscous fluid models for both classical and fractional cases, Stehfest and Tzou numerical methods are also employed to secure the validity of our solutions. Moreover, it is visualized that for a short time, temperature and momentum

Abbreviations: W_1, velocity $[ms^{-1}]$; β_1, volumetric coefficient of thermal expansion $[K^{-1}]$; g, acceleration due to gravity $[LT^{-2}]$; T_∞, temperature value away from the plate $[K]$; T_w, temperature on the plate $[K]$; C_∞, concentration value away from the plate $[kgm^{-3}]$; T, temperature $[K]$; C_w, concentration at the plate $[ML^{-3}]$; Gr, thermal Grashof number [-]; μ_{hbnf}, dynamic viscosity of hybrid nanofluid [-]; κ_{hbnf}, thermal conductivity of hybrid nanofluid [-]; Pr, Prandtl number [-]; λ_2, Maxwell parameter [-]; ϕ_1, ϕ_2, volumetric fractions [-]; Gm, mass Grashof number [-]; ρ_{hbnf}, density for hybrid nanofluid [-]; C_p, specific heat at constant pressure $[JM^{-1}K^{-1}]$; λ_1, Oldroyd parameter [-]; s, Laplace transformed variable [-]; α, γ, fractional parameters [-]. Note: this [-] characterizes the dimensionless quantity.

profiles are decayed for larger values of α, and this effect is reversed for a long time. Furthermore, the energy and velocity profiles are higher for water-based HNFs than those for the sodium alginate-based HNF.

KEYWORDS

fractionalized hybrid Oldroyd-B fluid, AB time-fractional derivative, Newtonian heating, Laplace transform method, hybrid nanofluid

1 Introduction

With the addition of nanometer-sized particles in various base fluids, thermophysical characteristics may improve in energy transfer schemes. This process signals an expansion in the thermal conductivity for base fluids, making it more reliable and ongoing. These significant fluids define nanofluids (NFs) with an extensive series of suggestions in several areas of science, as well as technology, with nuclear devices, heat exchangers, solar plates, vehicle heaters, and biotic and organic devices (Usman et al., 2018; Khan et al., 2022a; Khan et al., 2022b; Ahmed et al., 2022; Hassan et al., 2022; Khan et al., 2022c). First, Lee and Eastman presented the idea of NFs in 1995 (Lee et al., 1999). Numerous applications of NFs are discoursed by Kaufui et al. (Wong and Omar De Leon., 2010). Mahian et al. (2019) proposed important ideas and reflected novel innovations to completely explain the NFs. They were obsessed with innovative expansions in this field, comprehensive explanations of the thermophysical characteristics, and imitation of thermal transmission in NF flow. Waini et al. (2019) used a numerical scheme to discuss an unsteady thermal transmission flow past a shrinking sheet in an HNF. They presented different applications of NFs in numerous branches of science along with appreciated recommendations. NFs have achieved significant consideration from researchers due to their improved heat conversion characteristics. The rheological presentation of an NF using a revolving rheometer was proposed by Vallejo et al. (2019a). Different rheological characteristics of NFs are discussed in Vallejo et al. (2019b). Currently, NFs have been characterized as HNFs in several mechanisms (Rashad et al., 2018). HNFs are developed by mixing two dissimilar nanoparticles in the base liquid. Its main inspiration is to increase the thermal features of NFs. The variable thermal transmission of HNFs through magnetic influence was examined in Mohebbi et al. (2019). The heat transmission in the non-Newtonian HNF composed with entropy generation was discussed in Shahsavar et al., 2018). Furthermore, Farooq et al. (2018) deliberated on the entropy in the HNF flow in a stretching sheet.

Asogwa et al. (2021) discussed chemical reactions and heat sinks over a ramped temperature. The analytical solution of governing equations was found with the Laplace transform. Asogwa et al. (2022a) used the Laplace approach to discuss a water-based NF containing aluminum oxide and copper in a moving plate and proved that thermal absorption causes a decline in aluminum oxide NF's thermal and momentum profiles with a copper NF. Shankar Goud et al. (2022) used the Keller–box scheme for the numerical solution along with thermal effects, momentum, and solutal slip on the thermal transmission with a description of the magnetohydrodynamic (MHD) flow of Casson fluid and an exponential porous surface with Dufour, chemical reaction, and Soret impacts. Khan et al. (2022d) studied a fractionalized electro-osmotic flow based on the Caputo operator of a Casson NF containing sodium alginate nanoparticles over a vertical microchannel with MHD effects. They proved that the inclination angle boosts the velocity. Asogwa et al. (2022b) and Asogwa et al. (2022c) considered the stimulation significance of the thermal transmission with the MHD flow of a NF through an extending sheet with MATLAB bvp4c. Furthermore, they investigated the radiative features of the MHD flow with collective heat transportation characteristics on a reactive stretching surface with the Casson NF numerically using MATLAB bvp4c. Goud et al. (2022) applied the bvp4c scheme to study the convection flow *via* an infinite porous plate on thermal transmission, as well as mass transmission. Asogwa et al. (2022d) discussed the influences of the movement of nanoparticles in NFs by an exponentially enhanced Riga plate. Reddy et al. (2022) calculated the effect of activation energy on a second-grade MHD NF flow over a convectively curved heated stretched surface by considering the Brownian motion and generation/absorption, and thermophoresis. They have shown that velocity and thermal profiles suggestively increase with the concurrent increasing estimation of the fluid parameter.

The fractional calculus (FC) has obtained substantial consideration from experts in previous decades. The important inventions have newly been presented in the application of the FC, where new derivatives, as well as integral operators, are hired (Awan et al., 2019). The new anticipated operators contain the generalized Mittag–Leffler function (MLF), and these features intensify the innovative constructions to achieve numerous attractive properties that are recognized in important outcomes. Subsequently, Atangana and Dumitru (2016) anticipated, the innovative and applicable time-fractional operator, which is expansively hired in numerous branches of science and engineering. It is exposed that the MLF is a more operative and vigorous screening apparatus than the exponential and power laws, constructing the AB-fractional operator, in terms of Caputo, an effective arithmetic procedure to simulate progressively perilous complex tasks. Due to their extensive implications, such fractional models are extensively identified for deriving fractional differential equations (FDEs) with no manufactured irregularities, as for Caputo, Riemann–Liouville (RL), and Caputo–Fabrizio (CF) derivatives, because of their characteristic non-orientation (Ali et al., 2021; Ali et al., 2022a; Raza et al., 2022; Zhang et al., 2022). We also perceived interest in these fractional derivatives on the topic of mathematical approaches, although scientifically approximating these operators' outcomes to compute different problems (Martyushev and Sheremet, 2012; Ali et al., 2022b).

Batool et al. (2022) discussed the thermal and mass transmission processes of a micropolar NF under magnetic and buoyancy effects across an inclusion. Rasool et al. (2022a) examined the significance of the MHD Maxwell NF flow and obtained the solution to this problem by employing the homotopy analysis technique for diverse physical parameters. Moreover, they studied an electro-magneto-hydrodynamic NF flow in a permeable medium with heating

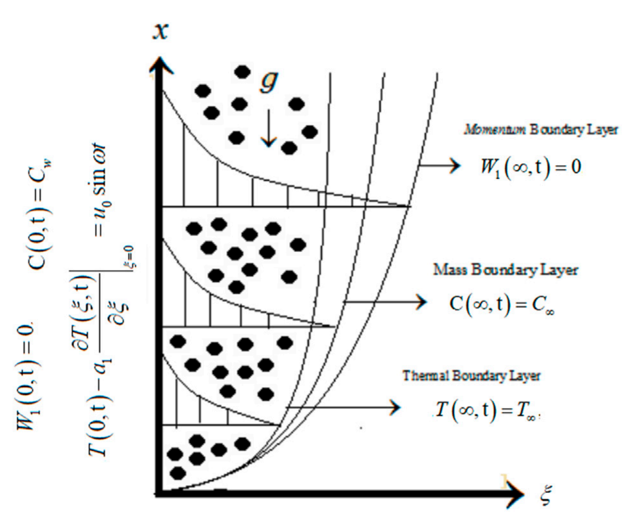

FIGURE 1
Physical flow.

boundary conditions. Furthermore, they applied Buongiorno's method for the flow of radiating thixotropic NFs over a horizontal surface by considering the retardational effects of Lorentz forces and using the influence of Brownian and thermophoresis diffusions (Rasool et al., 2022b; Rasool et al., 2023).

In this paper, a fractionalized Oldroyd-B HNF flow is examined by the recent definitions of the AB time-fractional derivative having a Mittage–Leffler kernel along with Newtonian heating, constant concentration, and the wall slip condition on temperature close to an infinite vertical flat plate. The AB fractional operator is introduced in the governing equations of temperature and diffusion by employing the generalized types of Fourier and Fick's law. The developed non-dimensional fractional model is solved using the Laplace transform method. Graphical illustrations are used to depict the physical behavior of fractional derivatives and the consequence of diverse flow parameters on velocity, thermal, and concentration fields. Furthermore, for validation of our attained results, some limiting cases are considered to recover fractional derivatives, as well as classical models of Maxwell and Newtonian fluids. The impacts of diverse flow parameters on variable profiles are achieved and presented graphically with significant conclusions.

2 Mathematical formulation based on a hybrid nanofluid

Consider an unsteady and an incompressible Oldroyd-B HNF flow close to an infinite vertical flat plate. Initially, consider that the fluid and plate are at a relaxation position, with constant temperature T_∞ and concentration C_∞. After some time, the plate is kept constant and the fluid begins to move with a temperature value $T(0,t)-a_1\frac{\partial T(0,t)}{\partial \xi}=u_0\sin\omega t$, where u_0 is a constant that signifies the dimension of velocity. At that time, the plate obtains a temperature T_w and concentration C_w, which persist constantly. We supposed that velocity, temperature, and concentration profiles are the only functions of ξ and t. The configuration of the problem is shown in Figure 1.

By Boussinesq's estimation (Ali et al., 2021), the governing equations for an Oldroyd-B HNF are discussed by Martyushev and Sheremet (2012). The equation of motion is as follows:

$$\begin{aligned}\rho_{hbnf}\left(1+\lambda_1\frac{\partial}{\partial t}\right)\frac{\partial W_1(\xi,t)}{\partial t}&=\mu_{hbnf}\left(1+\lambda_2\frac{\partial}{\partial t}\right)\frac{\partial^2 W_1(\xi,t)}{\partial \xi^2}\\&+g(\rho\beta_1)_{hbnf}\left(1+\lambda_1\frac{\partial}{\partial t}\right)\\&\times(T(\xi,t)-T_\infty)\\&+g(\rho\beta_2)_{hbnf}\left(1+\lambda_1\frac{\partial}{\partial t}\right)\\&\times(C(\xi,t)-C_\infty).\end{aligned}\tag{1}$$

The energy balance equation is as follows (Awan et al., 2019):

$$\left(\rho C_p\right)_{hbnf}\frac{\partial T(\xi,t)}{\partial t}=-\frac{\partial q}{\partial \xi}.\tag{2}$$

The Fourier law (Zhang et al., 2022) for thermal conduction is as follows:

$$q(\xi,t)=-\kappa_{hbnf}\frac{\partial T(\xi,t)}{\partial \xi}.\tag{3}$$

The diffusion equation (Awan et al., 2019) for

$$\frac{\partial C(\xi,t)}{\partial t}=-\frac{\partial j}{\partial \xi}.\tag{4}$$

The Fick law is as follows (Awan et al., 2019):

$$j(\xi,t)=-D_{hbnf}\frac{\partial C(\xi,t)}{\partial \xi}.\tag{5}$$

The appropriate initial and boundary conditions are as follows:

$$W_1(\xi,0)=0, T(\xi,0)=T_\infty, C(\xi,0)=C_\infty, \forall\xi\geq 0,\tag{6}$$

$$W_1(0,t)=0, T(0,t)-a_1\frac{\partial T(\xi,t)}{\partial \xi}\bigg|_{\xi=0}=u_0\sin\omega t, C(0,t)=C_w,\tag{7}$$

$$W_1(\xi,t)\to 0, T(\xi,t)\to T_\infty, C(\xi,t)\to C_\infty \text{ as}, \xi\to\infty .\tag{8}$$

Table 1 shows the properties of thermal and under-conversation fluids and nanoparticles.

$$\begin{aligned}\rho_{hbnf}&=\rho_f(1-\phi_2)\times\left(\frac{\rho_{s_1}}{\rho_f}\phi_1+(1-\phi_1)\right)+\phi_2\rho_{s_2}\mu_{hbnf}\\&=\frac{\mu_f}{(1-\phi_1)^{2.5}(1-\phi_2)^{2.5}},\left(\rho C_p\right)_{hbnf}=\left(\rho C_p\right)_f(1-\phi_2)\\&\times\left((1-\phi_1)+\phi_1\frac{(\rho C_p)_{s_1}}{(\rho C_p)_f}\right)+\phi_2\left(\rho C_p\right)_{s_2},(\rho\beta_T)_{hbnf}\\&=(1-\phi_2)(\rho\beta_T)_f\times\left((1-\phi_1)+\phi_1\frac{(\rho\beta_T)_{s_1}}{(\rho\beta_T)_f}\right)\\&+\phi_2(\rho\beta_T)_{s_2},\kappa_{hbnf}=\left(\frac{\kappa_{s_2}+(s-1)\kappa_{bf}-(s-1)\phi_2\left(\kappa_{bf}-\kappa_{s_2}\right)}{\kappa_{s_2}+(s-1)\kappa_{bf}+\phi_2\left(\kappa_{bf}-\kappa_{s_2}\right)}\right)\kappa_{bf},\kappa_{bf}\\&=\left(\frac{\kappa_{s_1}+(s-1)\kappa_f-(s-1)\phi_1\left(\kappa_f-\kappa_{s_1}\right)}{\kappa_{s_1}+(s-1)\kappa_f+\phi_1\left(\kappa_f-\kappa_{s_1}\right)}\right)\kappa_f.\end{aligned}\tag{9}$$

TABLE 1 Thermal characteristics of base fluids and nanoparticles (Raza et al., 2022; Zhang et al., 2022).

Material	Water (H_2O)	Sodium alginate $(C_6H_9NaO_7)$	Aluminum oxide (Al_2O_3)	Ferro-ferric oxide (Fe_3O_4)
$\rho(M/L^3)$	997.1	898	3970	5180
$C_p(J/M\,K)$	4179	4175	765	670
$k(W/L\,K)$	0.613	0.6367	40	9.7
$\beta_T(K^{-1})$	21	23	0.85	0.9
σ	0.05	0.07	3.6×10^7	1×10^{-7}

The properties of a HNF are defined by Zhang et al. (2022).

TABLE 2 Numerical comparison of energy, concentration, and velocity profiles by different numerical methods.

ψ	$\theta(\psi,\eta)$ by Stehfest	$\theta(\psi,\eta)$ by Tzou	$\Phi(\psi,\eta)$ by Stehfest	$\Phi(\psi,\eta)$ by Tzou	$\mathbf{W}(\psi,\eta)$ by Stehfest	$\mathbf{W}(\psi,\eta)$ by Tzou
0.1	0.61263	0.61309	0.97297	0.9736	0.15292	0.15291
0.5	0.45242	0.45274	0.87168	0.87198	0.60469	0.60453
0.9	0.33289	0.33311	0.78055	0.7806	0.86701	0.86664
1.3	0.24413	0.24428	0.6986	0.69848	1.0032	1.0026
1.7	0.17849	0.1786	0.62496	0.62473	1.0553	1.0546
2.1	0.13014	0.13021	0.55882	0.55852	1.0522	1.0515
2.5	0.094641	0.094686	0.49946	0.49911	1.0137	1.0129
2.9	0.068661	0.06869	0.44621	0.44584	0.95349	0.95272
3.3	0.049701	0.04972	0.39847	0.39809	0.88123	0.8805
3.7	0.035902	0.035914	0.35568	0.35532	0.80356	0.80288
4.1	0.025884	0.025891	0.31737	0.31702	0.7 2499	0.72437
4.5	0.018627	0.018631	0.28306	0.28274	0.64852	0.64796
4.9	0.013381	0.013384	0.25237	0.25207	0.57605	0.57556

The following are a set of non-dimensional parameters:

$$\psi^* = \frac{u_0}{v_f}\xi, \eta^* = \frac{u_0^2}{v_f}\mathrm{t}, W^* = \frac{W_1}{u_0}, \theta^* = \frac{T-T_\infty}{T_w-T_\infty}, \Phi^* = \frac{C-C_\infty}{C_w-C_\infty}, \mathrm{q}^* = \frac{q}{q_0}, \mathrm{j}^* = \frac{j}{j_0},$$
$$\lambda_1^* = \frac{u_0^2}{v_f}\lambda_1, \lambda_2^* = \frac{u_0^2}{v_f}\lambda_2, q_0 = \frac{\kappa_f(T_w-T_\infty)u_0}{v_f}, \mathrm{j}_0 = \frac{D_{nf}(C_w-C_\infty)u_0}{v_f},$$
$$Gr = \frac{g(v\beta_1)_f(T_w-T_\infty)}{u_0^3}, Gm = \frac{g(v\beta_2)_f(C_w-C_\infty)}{u_0^3}, \mathrm{Pr} = \frac{(\mu C_P)_f}{\kappa_f}, Sc = \frac{v_f}{D_f}. \tag{10}$$

By utilizing the aforementioned variables in Eqs. 1–8 and after dropping the * notation, we obtain

$$\Omega_1\left(1+\lambda_1\frac{\partial}{\partial\eta}\right)\frac{\partial W(\psi,\eta)}{\partial\eta} = \Omega_2\left(1+\lambda_2\frac{\partial}{\partial\eta}\right)\frac{\partial^2 W(\psi,\eta)}{\partial\psi^2} + \Omega_3\left(1+\lambda_1\frac{\partial}{\partial\eta}\right)Gr\,\theta(\psi,\eta) + \Omega_4\left(1+\lambda_1\frac{\partial}{\partial\eta}\right)Gm\,\Phi(\psi,\eta). \tag{11}$$

$$\Omega_5\mathrm{Pr}\frac{\partial\theta(\psi,\eta)}{\partial\eta} = -\frac{\partial q}{\partial\psi}. \tag{12}$$

$$q(\psi,\eta) = -\Omega_6\frac{\partial\theta(\psi,\eta)}{\partial\psi}. \tag{13}$$

$$^{AB}D_\eta^\alpha\Phi(\psi,\eta) = -\frac{(1-\phi_1)(1-\phi_2)}{Sc}\frac{\partial j}{\partial\psi}, \tag{14}$$

$$j(\psi,\eta) = -\frac{\partial\Phi(\psi,\eta)}{\partial\psi}. \tag{15}$$

$$W(\psi,0) = 0, \theta(\psi,0) = 0, \Phi(\psi,0) = 0, \forall\psi\geq 0, \tag{16}$$

$$W(0,\eta) = 0, \theta(0,\eta) - a_1\frac{\partial\theta(\psi,\eta)}{\psi}\bigg|_{\psi=0} = \sin\omega\eta, \Phi(0,\eta) = 1, \forall\eta>0, \tag{17}$$

$$W(\psi,\eta)\to 0, \theta(\psi,\eta)\to 0, \Phi(\psi,\eta)\to 0, \mathrm{as}, \psi\to\infty\,. \tag{18}$$

where

$$\Omega_1 = (1-\phi_2)\times\left((1-\phi_1)+\phi_1\frac{\rho_{s_1}}{\rho_f}\right)+\phi_2\frac{\rho_{s_2}}{\rho_f}, \Omega_2 = \frac{1}{(1-\phi_1)^{2.5}(1-\phi_2)^{2.5}},$$
$$\Omega_3 = (1-\phi_2)\times\left((1-\phi_1)+\phi_1\frac{(\rho\beta_1)_{s_1}}{(\rho\beta_1)_f}\right)+\phi_2\frac{(\rho\beta_1)_{s_2}}{(\rho\beta_1)_f},$$
$$\Omega_4 = (1-\phi_2)\times\left((1-\phi_1)+\phi_1\frac{(\rho\beta_2)_{s_2}}{(\rho\beta_2)_f}\right)+\phi_2\frac{(\rho\beta_2)_{s_2}}{(\rho\beta_2)_f},$$
$$\Omega_5 = (1-\phi_2)\times\left((1-\phi_1)+\phi_1\frac{(\rho C_p)_s}{(\rho C_p)_f}\right)+\phi_2\frac{(\rho C_p)_{s_2}}{(\rho C_p)_f},$$
$$\Omega_6 = \left(\frac{\kappa_{s_2}+(s-1)\kappa_{bf}-(s-1)\phi_2(\kappa_{bf}-\kappa_{s2})}{\kappa_{s_2}+(s-1)\kappa_{bf}+\phi_2(\kappa_{bf}-\kappa_s)}\right)\kappa_{bf},$$
$$\kappa_{bf} = \left(\frac{\kappa_{s_1}+(s-1)\kappa_f-(s-1)\phi_1(\kappa_f-\kappa_{s_1})}{\kappa_{s_1}+(s-1)\kappa_f+\phi_1(\kappa_f-\kappa_{s_1})}\right). \tag{19}$$

2.1 Fractional model based on a non-local kernel

Now, we develop a fractional Oldroyd-B HNF using Fourier and Fick's law based on the AB-fractional operator (Atangana and Dumitru, 2016), which is explained as the following expression for a function $f(\xi,t)$

$$^{AB}D_t^{\gamma}f(\xi,t) = \frac{1}{1-\gamma}\int_0^t E_\gamma\left[\frac{\gamma(t-\tau)^\gamma}{1-\gamma}\right]f'(\xi,\tau)d\tau, 0<\gamma<1, \tag{20}$$

and the kernel Mittage–Leffler function $E_\gamma(\tau)$ is defined by

$$E_\gamma(\tau) = \sum_{r=0}^{\infty}\frac{\tau^\gamma}{\Gamma(r\gamma+1)}, 0<\gamma<1, \tau\in\mathbb{C}. \tag{21}$$

The Laplace transform is

$$L\{^{AB}D_t^\gamma f(\xi,t)\} = \frac{s^\gamma L\{f(\xi,t)\}-s^{\gamma-1}f(\xi,0)}{s^\gamma(1-\gamma)+\gamma}, \tag{22}$$

with

$$\lim_{\gamma\longrightarrow 1}{}^{AB}D_t^\gamma f(\xi,t) = \frac{\partial f(\xi,t)}{\partial t}. \tag{23}$$

The governing equations for the AB-fractional derivative are obtained by substituting the ordinary derivative with the AB derivative operator $^{AB}D_\eta^\alpha$ in Eqs. 11–15 as

$$\Omega_1\left(1+\lambda_1\frac{\partial}{\partial\eta}\right){}^{AB}D_\eta^\alpha W(\psi,\eta) = \Omega_2\left(1+\lambda_2\frac{\partial}{\partial\eta}\right)\frac{\partial^2 W(\psi,\eta)}{\partial\psi^2}$$
$$+\Omega_3\left(1+\lambda_1\frac{\partial}{\partial\eta}\right)Gr\ \theta(\psi,\eta)+\Omega_4\left(1+\lambda_1\frac{\partial}{\partial\eta}\right)Gm\ \Phi(\psi,\eta), \tag{24}$$

$$\Omega_5\Pr{}^{AB}D_\eta^\alpha\theta(\psi,\eta) = -\frac{\partial q}{\partial\psi}, \tag{25}$$

$$q(\psi,\eta) = -\Omega_6\frac{\partial\theta(\psi,\eta)}{\partial\psi}. \tag{26}$$

$$^{AB}D_\eta^\alpha\Phi(\psi,\eta) = -\frac{1}{Sc}\frac{\partial j}{\partial\psi}, \tag{27}$$

$$j(\psi,\eta) = -\frac{\partial\Phi(\psi,\eta)}{\partial\psi}. \tag{28}$$

3 Solution of the problem

3.1 Energy profile

Using the Laplace transform on Eqs. 25, 26 and corresponding conditions $(15)_2$-$(17)_2$, we have

$$\Omega_6\Pr\left(\frac{s^\alpha}{(1-\alpha)s^\alpha+\alpha}\right)\bar\theta(\psi,s) = -\frac{\partial\bar q}{\partial\psi}, \tag{29}$$

$$\bar q(\psi,s) = -\Omega_6\frac{\partial\bar\theta(\psi,s)}{\partial\psi}, \tag{30}$$

$$\bar\theta(0,s)-a_1\frac{\partial\bar\theta(\psi,s)}{\psi}\Big|_{\psi=0} = \frac{\omega}{s^2+\omega^2},$$
$$\bar\theta(\psi,s)\to 0, \text{as}, \psi\to\infty, \tag{31}$$

where $\bar\theta(\psi,s) = \int_0^\infty\theta(\psi,t)e^{-st}dt$ is the Laplace transform for $\theta(\psi,t)$, and s is the Laplace transform parameter (Ali et al., 2021).

The solution of Eq. (29) by using Eq. (30) and with conditions in Eq. (31) is

$$\bar\theta(\psi,s) = \frac{\omega}{(s^2+\omega^2)}\frac{1}{1+a\sqrt{\frac{\Pi s^\alpha}{(1-\alpha)s^\alpha+\alpha}}}\exp\left(-\psi\sqrt{\frac{\Pi s^\alpha}{(1-\alpha)s^\alpha+\alpha}}\right). \tag{32}$$

Eq. (32) can be written as

$$\bar\theta(\psi,s) = \frac{\omega}{(s^2+\omega^2)}\frac{1}{1+a\sqrt{\Lambda_1(s)}}\exp\left(-\psi\sqrt{\Lambda_1(s)}\right), \tag{33}$$

where $\Pi = \frac{\Omega_5\Pr}{\Omega_6}$ and $\Lambda_1(s) = \frac{\Pi s^\alpha}{(1-\alpha)s^\alpha+\alpha}$.

The Laplace inverse of Eq. (33) is shown numerically in Table 2.

3.2 Concentration field

By employing the Laplace transform on Eqs. 27, 28 with associated conditions defined in Eqs. $(15)_3$– $(17)_3$, we have

$$\frac{s^\alpha}{(1-\alpha)s^\alpha+\alpha}\bar\Phi(\psi,s) = -\frac{(1-\phi_1)(1-\phi_2)}{Sc}\frac{\partial\bar j(\psi,s)}{\partial\psi}, \tag{34}$$

$$\bar j(\psi,s) = -\frac{\partial\bar j(\psi,s)}{\partial\psi}. \tag{35}$$

$$\bar\Phi(0,s) = \frac{1}{s}, \bar\Phi(\psi,s)\to 0, \text{as}, \psi\to\infty\ . \tag{36}$$

The solution of Eq. (34) by using Eq. (35) and conditions in Eq. (36) is

$$\bar\Phi(\psi,s) = \frac{1}{s}\exp\left(-\psi\sqrt{\frac{Sc}{(1-\phi_1)(1-\phi_2)}\left(\frac{s^\alpha}{(1-\alpha)s^\alpha+\alpha}\right)}\right). \tag{37}$$

Eq. (37) may be written as

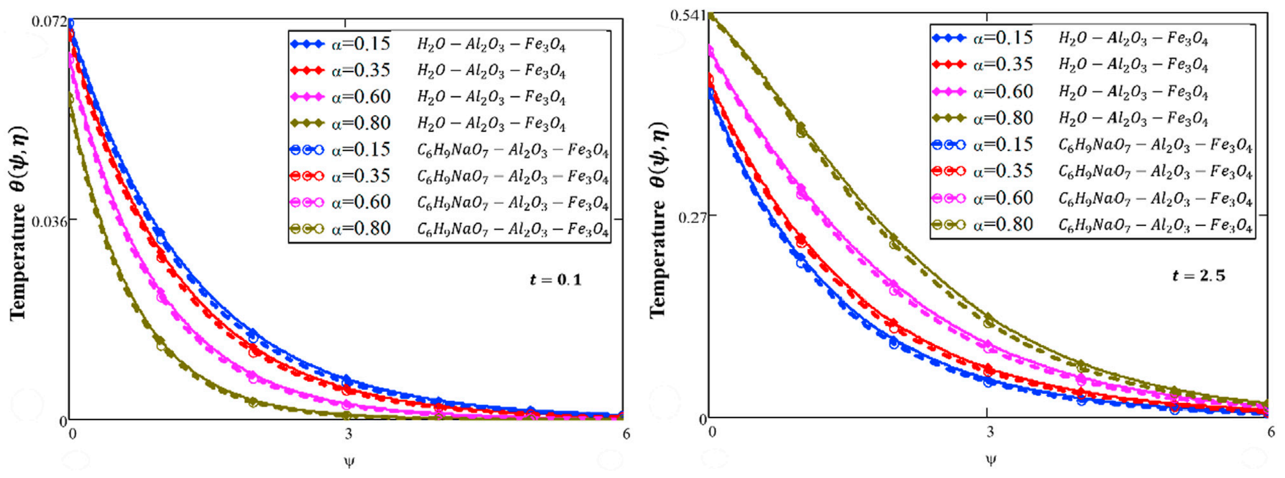

FIGURE 2
Simulation to explain the temperature for changing α when $Pr = 3$ and $\phi_1 = \phi_2 = 0.4$.

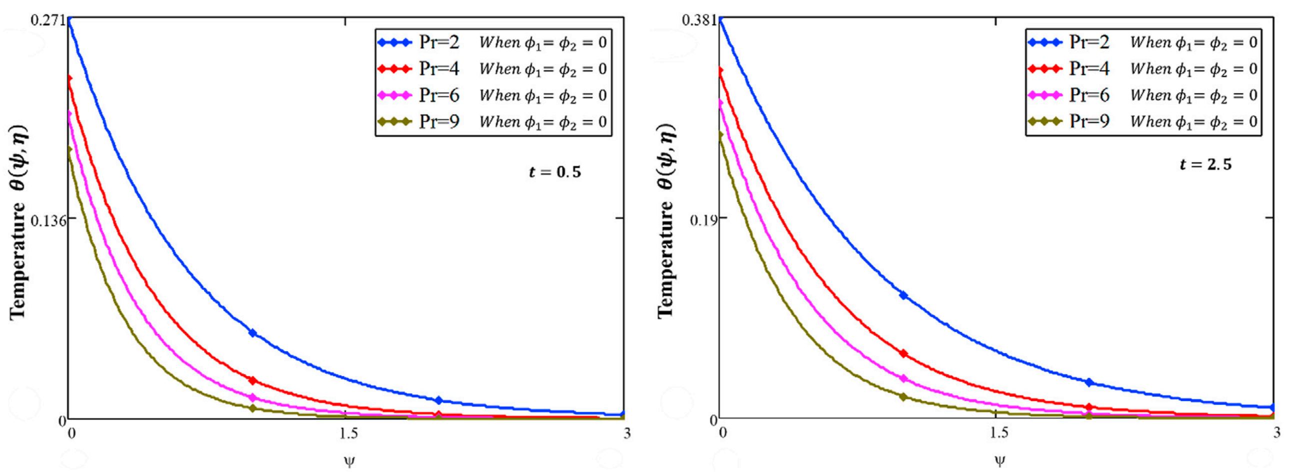

FIGURE 3
Simulation to explain the temperature for Pr when $\alpha = 0.4$.

$$\bar{\Phi}(\psi,s)=\frac{1}{s}\exp\left(-\psi\sqrt{\Lambda_2(s)}\right), \tag{38}$$

where $\Lambda_2(s)=\frac{Sc}{(1-\phi_1)(1-\phi_2)}\left(\frac{s^\alpha}{(1-\alpha)s^\alpha+\alpha}\right)$.

The Laplace inverse of Eq. (38) is computed numerically in Table 2 by invoking diverse numerical methods.

3.3 Momentum profile

Taking the Laplace transform on Eq. (24) with related conditions in Eqs. $(15)_1$– $(17)_1$, we have

$$\Omega_1(1+\lambda_1 s)\left(\frac{q^\alpha}{(1-\alpha)q^\alpha+\alpha}\right)\bar{W}(\psi,s)=\Omega_2(1+\lambda_2 s)\frac{\partial^2\bar{W}(\psi,s)}{\partial\psi^2}$$
$$+\Omega_3(1+\lambda_1 s)Gr\bar{\theta}(\psi,s)+\Omega_4(1+\lambda_1 s)Gm\bar{\Phi}(\psi,s), \tag{39}$$

$$\bar{W}(0,s)=0,\bar{W}(\psi,s)\to 0,\text{as},\psi\to\infty\,. \tag{40}$$

By using temperature values from Eq. (37) and concentration from Eq. (38) and with conditions of Eq. (40), we obtain the solution of the velocity field for Eq. (40) as

$$\bar{W}(\psi,s)=\frac{\Lambda_4(s)Gr}{\Lambda_3(s)-\Lambda_1(s)}\frac{\omega}{s^s+\omega^2}\left[\frac{e^{-\psi\sqrt{\Lambda_1(s)}}}{1+a\sqrt{\Lambda_1(s)}}-\frac{e^{-\psi\sqrt{\Lambda_3(s)}}}{1+a\sqrt{\Lambda_1(s)}}\right]$$
$$+\frac{\Lambda_5(s)Gm}{\Lambda_3(s)-\Lambda_2(s)}\left[\frac{e^{-\psi\sqrt{\Lambda_2(s)}}}{s}-\frac{e^{-\psi\sqrt{\Lambda_3(s)}}}{s}\right], \tag{41}$$

where
$b_1=\frac{1+\lambda_1 s}{1+\lambda_2 s}$, $\Lambda_3(s)=b_1\frac{\Omega_1}{\Omega_2}\frac{s^\alpha}{(1-\alpha)s^\alpha+\alpha}$, $\Lambda_4(s)=b_1\frac{\Omega_3}{\Omega_2}$, and $\Lambda_5(s)=b_1\frac{\Omega_4}{\Omega_2}$.

Our achieved solutions of variable profiles are complex to find analytically. Different researchers employed varied numerical approaches; so to compute Laplace inversion, we

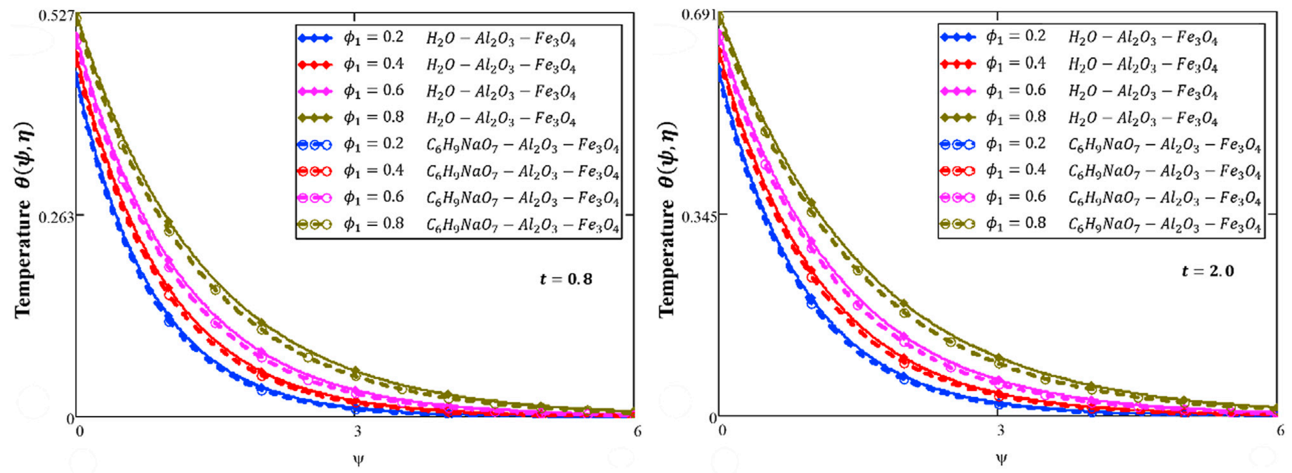

FIGURE 4
Simulation to explain the temperature for fluctuating ϕ_1 when $Pr = 6, \alpha = 0.4, and\, \phi_2 = 0.5$.

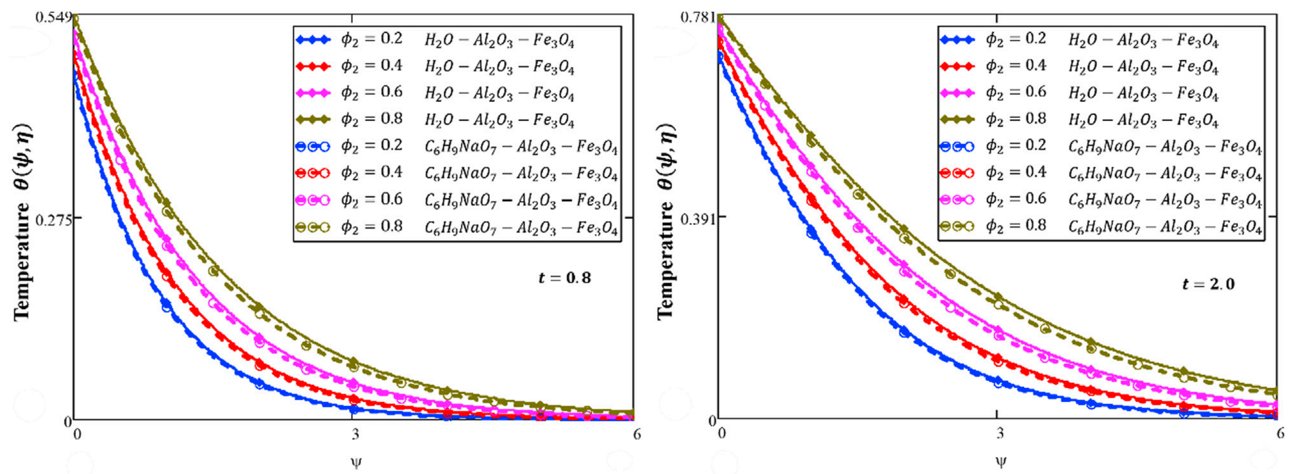

FIGURE 5
Simulation to explain the temperature for changing ϕ_2 when $Pr = 2, \alpha = 0.8, and\, \phi_1 = 0.2$.

also employed numerical techniques, i.e., Stehfest and Tzou numerical methods. These algorithms are defined as follows (Stehfest, 1970; Tzou, 2014):

$$W(\psi,\eta) = \frac{\ln(2)}{\eta}\sum_{m=1}^{M} w_m \bar{W}\left(\psi, \mathrm{m}\frac{\ln(2)}{\eta}\right), \tag{42}$$

where $w_m = (-1)^{m+\frac{M}{2}} \sum_{r=\left(\frac{q+1}{2}\right)}^{\min\left(q,\frac{M}{2}\right)} \frac{r^{\frac{M}{2}}(2r)!}{\left(\frac{M}{2}-r\right)!r!(r-1)!(q-r)!(2r-q)!}$,

and

$$W(\psi,\eta) = \frac{e^{4.7}}{\eta}\left[\frac{1}{2}\bar{W}\left(\psi,\frac{4.7}{\eta}\right) + \mathrm{Re}\left\{\sum_{j=1}^{M}(-1)^j \bar{W}\left(\psi,\frac{4.7+j\pi i}{\eta}\right)\right\}\right]. \tag{43}$$

Case I. Classical Oldroyd-B fluid

Bysubstituting$\alpha = 1$inEq.(41),thevelocitysolutiontakestheformas

$$\bar{W}(\psi,s) = \frac{\Omega_3\Omega_6(1+\lambda_1 s)Gr}{\Omega_1\Omega_6(1+\lambda_1 s) - \Omega_2\Omega_5\mathrm{Pr}(1+\lambda_2 s)}\frac{\omega}{s^2+\omega^2}\left[\frac{e^{-\psi\sqrt{s\frac{\Omega_5\mathrm{Pr}}{\Omega_6}}}}{1+a\sqrt{s\frac{\Omega_5\mathrm{Pr}}{\Omega_6}}} - \frac{e^{-\psi\sqrt{\frac{1+\lambda_1 s}{1+\lambda_2 s}\frac{\Omega_1}{\Omega_2}s}}}{1+a\sqrt{s\frac{\Omega_5\mathrm{Pr}}{\Omega_6}}}\right] + \frac{\Omega_4 Sc(1+\lambda_1 s)Gm}{\Omega_1 Sc(1+\lambda_1 s) - \Omega_2(1+\lambda_2 s)}\left[\frac{e^{-\psi\sqrt{\frac{s}{Sc}}}}{s} - \frac{e^{-\psi\sqrt{\frac{1+\lambda_1 s}{1+\lambda_2 s}\frac{\Omega_1}{\Omega_2}s}}}{s}\right]. \tag{44}$$

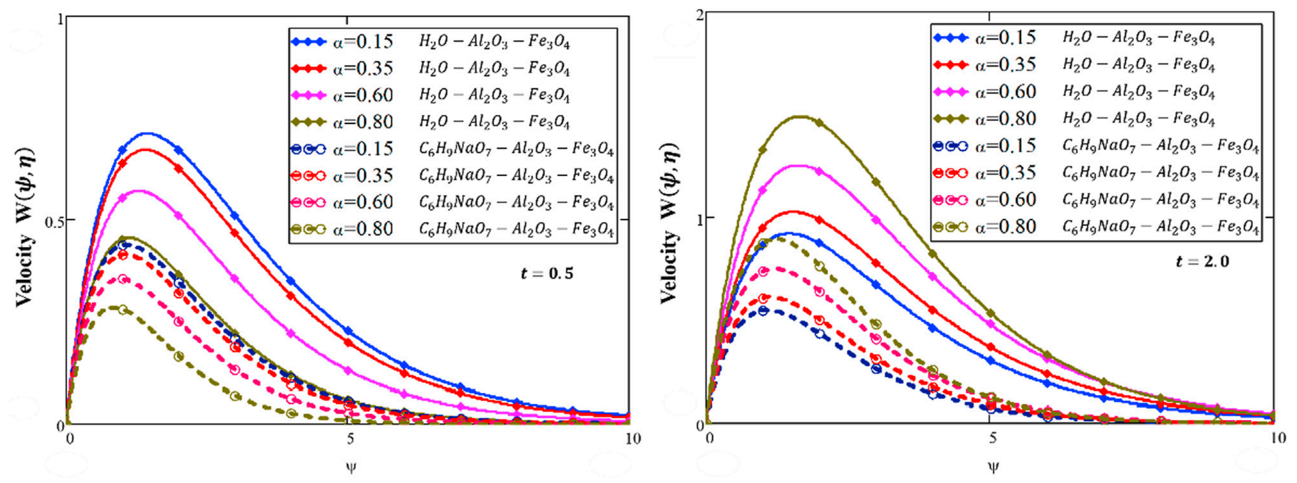

FIGURE 6
Simulation to explain the velocity for fluctuating α when $Pr = 3.2, \phi_1 = \phi_2 = 0.2, Gr = 8, Gm = 6.5, Sc = 0.5, \lambda_1 = 0.5$, and $\lambda_1 = 0.5$.

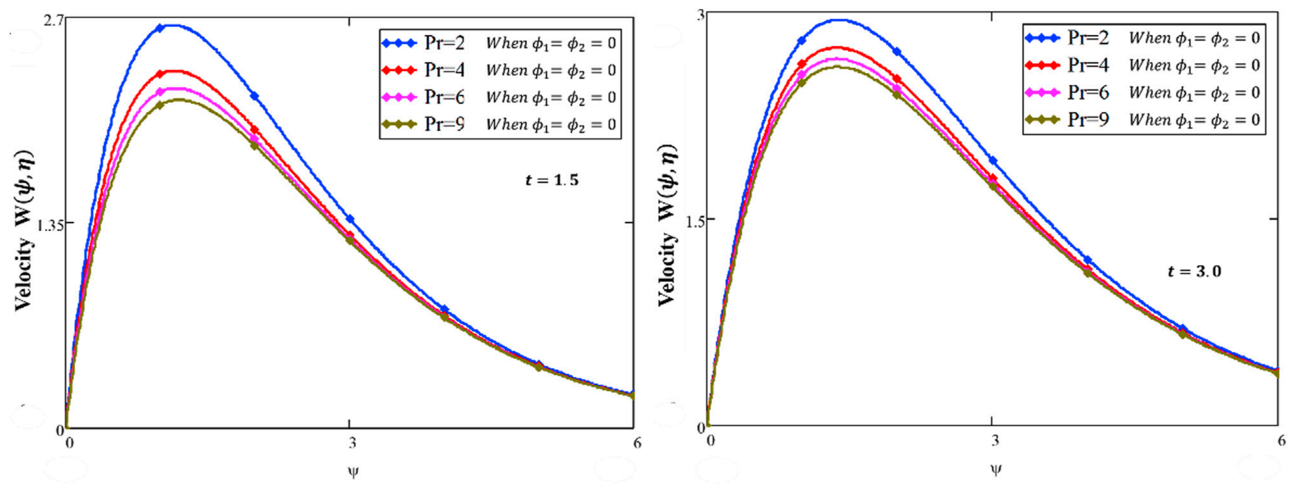

FIGURE 7
Simulation to explain the velocity for changing Pr when $\alpha = 0.5, Gr = 8, Gm = 6.5, Sc = 0.5, \lambda_1 = 0.5$, and $\lambda_1 = 0.3$.

Case II. Fractionalized Maxwell fluid

By substituting $\lambda_2 = 0$ in Eq. (41), the velocity solution converts as follows:

$$\bar{W}(\psi,s)=\frac{(1+\lambda_1 s)\left((1-\alpha)s^\alpha+\alpha\right)\Omega_3\Omega_6 Gr}{(1+\lambda_1 s)\Omega_1\Omega_6 s^\alpha-\Omega_5\Omega_2 \Pr s^\alpha}\frac{\omega}{s^s+\omega^2}\frac{1}{1+a\sqrt{\frac{\Omega_5\Pr}{\Omega_6}\frac{s^\alpha}{(1-\alpha)s^\alpha+\alpha}}}\left(e^{-\psi\sqrt{\frac{\Omega_5\Pr}{\Omega_6}\frac{s^\alpha}{(1-\alpha)s^\alpha+\alpha}}}-e^{-\psi\sqrt{(1+\lambda_1 s)\frac{\Omega_1}{\Omega_2}\frac{s^\alpha}{(1-\alpha)s^\alpha+\alpha}}}\right)+\frac{(1+\lambda_1 s)\left((1-\alpha)s^\alpha+\alpha\right)\Omega_4 ScGm}{(1+\lambda_1 s)\Omega_1 Scs^\alpha-\Omega_2 s^\alpha}\left(\frac{e^{-\psi\sqrt{\frac{1}{Sc}\left(\frac{s^\alpha}{(1-\alpha)s^\alpha+\alpha}\right)}}}{s}-\frac{e^{-\psi\sqrt{(1+\lambda_1 s)\frac{\Omega_1}{\Omega_2}\frac{s^\alpha}{(1-\alpha)s^\alpha+\alpha}}}}{s}\right). \tag{45}$$

Case III. Ordinary Maxwell fluid

By substituting $\alpha = 1$ and $\lambda_2 = 0$ in Eq. (41), the velocity solution converts

$$\bar{W}(\psi,s)=\frac{(1+\lambda_1 s)\Omega_3\Omega_6 Gr}{(1+\lambda_1 s)\Omega_1\Omega_6-\Omega_5\Omega_2\Pr}\frac{\omega}{s^2+\omega^2}\frac{1}{1+a\sqrt{s\frac{\Omega_5\Pr}{\Omega_6}}}\left[e^{-\psi\sqrt{s\frac{\Omega_5\Pr}{\Omega_6}}}-e^{-\psi\sqrt{(1+\lambda_1 s)\frac{\Omega_1}{\Omega_2}s}}\right]+\frac{(1+\lambda_1 s)\Omega_4 ScGm}{(1+\lambda_1 s)\Omega_1 Sc-\Omega_2}\left[\frac{e^{-\psi\sqrt{\frac{s}{Sc}}}}{s}-\frac{e^{-\psi\sqrt{(1+\lambda_1 s)\frac{\Omega_1}{\Omega_2}s}}}{s}\right]. \tag{46}$$

Case IV. Fractionalized Newtonian fluid

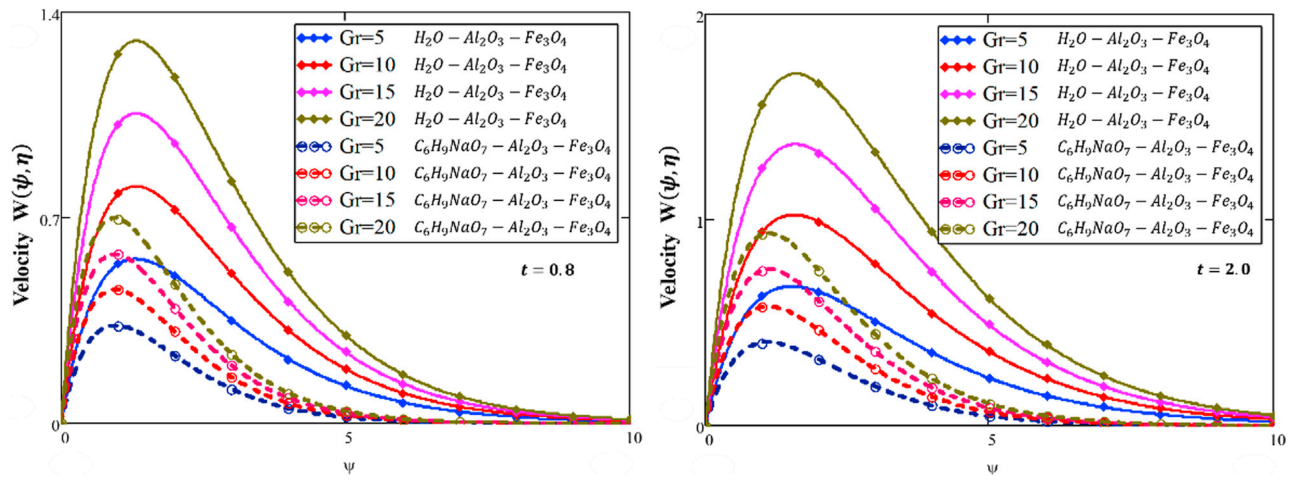

FIGURE 8
Simulation to explain the velocity for changing Gr when $\alpha = 0.4, Pr = 2.5, \phi_1 = \phi_2 = 0.2, Gm = 4.5, Sc = 0.8, \lambda_1 = 0.7, and\, \lambda_1 = 0.3$.

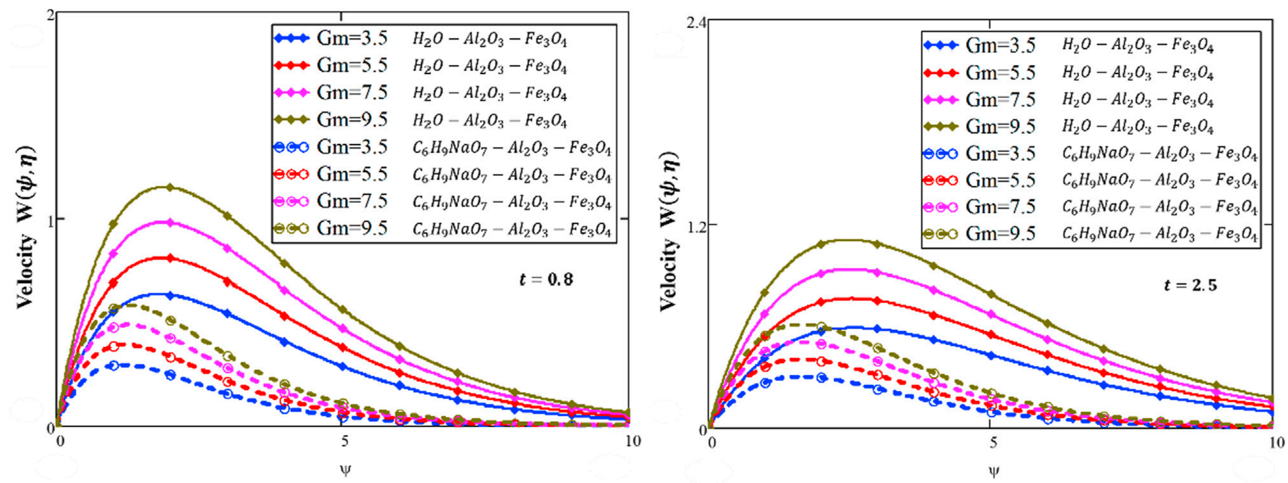

FIGURE 9
Simulation to explain the velocity for changing Gm when $\alpha = 0.4, Pr = 3.2, \phi_1 = \phi_2 = 0.3, Gr = 8, Sc = 0.2, \lambda_1 = 1.2, and\, \lambda_1 = 0.3$.

By substituting $\lambda_1 = 0$ in Eq. (45), the velocity solution converts

$$\bar{W}(\psi,s)=\frac{((1-\alpha)s^\alpha+\alpha)\Omega_3\Omega_6 Gr}{\Omega_1\Omega_6 s^\alpha-\Omega_5\Omega_2 \Pr s^\alpha}\frac{\omega}{s^s+\omega^2}\frac{1}{1+a\sqrt{\frac{\Omega_5\Pr}{\Omega_6}\frac{s^\alpha}{(1-\alpha)s^\alpha+\alpha}}}\left[e^{-\psi\sqrt{\frac{\Omega_5\Pr}{\Omega_6}\frac{s^\alpha}{(1-\alpha)s^\alpha+\alpha}}}-e^{-\psi\sqrt{\frac{\Omega_1}{\Omega_2}\frac{s^\alpha}{(1-\alpha)s^\alpha+\alpha}}}\right]+\frac{((1-\alpha)s^\alpha+\alpha)\Omega_4 ScGm}{\Omega_1 Scs^\alpha-\Omega_2 s^\alpha}\left[\frac{e^{-\psi\sqrt{\frac{1}{Sc}\left(\frac{s^\alpha}{(1-\alpha)s^\alpha+\alpha}\right)}}}{s}-\frac{e^{-\psi\sqrt{\frac{\Omega_1}{\Omega_2}\frac{s^\alpha}{(1-\alpha)s^\alpha+\alpha}}}}{s}\right]. \quad (47)$$

Case V. Ordinary Newtonian fluid

By substituting $\alpha = 1$ in Eq. (47), the velocity solution converts

$$\bar{W}(\psi,s)=\frac{\Omega_3\Omega_6 Gr}{\Omega_1\Omega_6-\Omega_5\Omega_2\Pr}\frac{\omega}{s^s+\omega^2}\frac{1}{1+a\sqrt{\frac{\Omega_5\Pr}{\Omega_6}}}\left[e^{-\psi\sqrt{\frac{\Omega_5\Pr}{\Omega_6}}}-e^{-\psi\sqrt{\frac{\Omega_1}{\Omega_2}}}\right]+\frac{\Omega_4 ScGm}{\Omega_1 Sc-\Omega_2}\left[\frac{e^{-\psi\sqrt{\frac{1}{Sc}}}}{s}-\frac{e^{-\psi\sqrt{\frac{\Omega_1}{\Omega_2}}}}{s}\right]. \quad (48)$$

4 Discussion of results

In this article, the natural convection flow of the Oldroyd-B HNF flowing close to an infinite vertical flat plate is examined. Aluminum oxide–magnetite–water (Al_2O_3–Fe_3O_4–H_2O) and aluminum oxide–magnetite–sodium alginate (Al_2O_3–Fe_3O_4–$C_6H_9NaO_7$)-based HNFs are considered with an AB-fractional approach. The

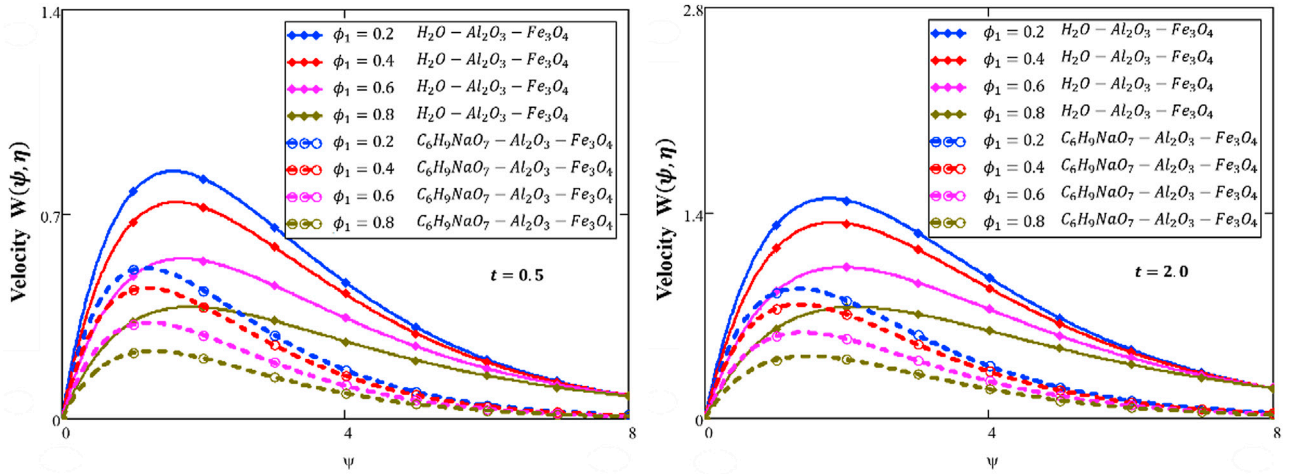

FIGURE 10
Simulation to explain the velocity for fluctuating ϕ_1 when $\alpha = 0.5, Pr = 3.2, \phi_2 = 0.3, Gr = 6, Gm = 8, Sc = 0.3, \lambda_1 = 0.7$, and $\lambda_1 = 1$.

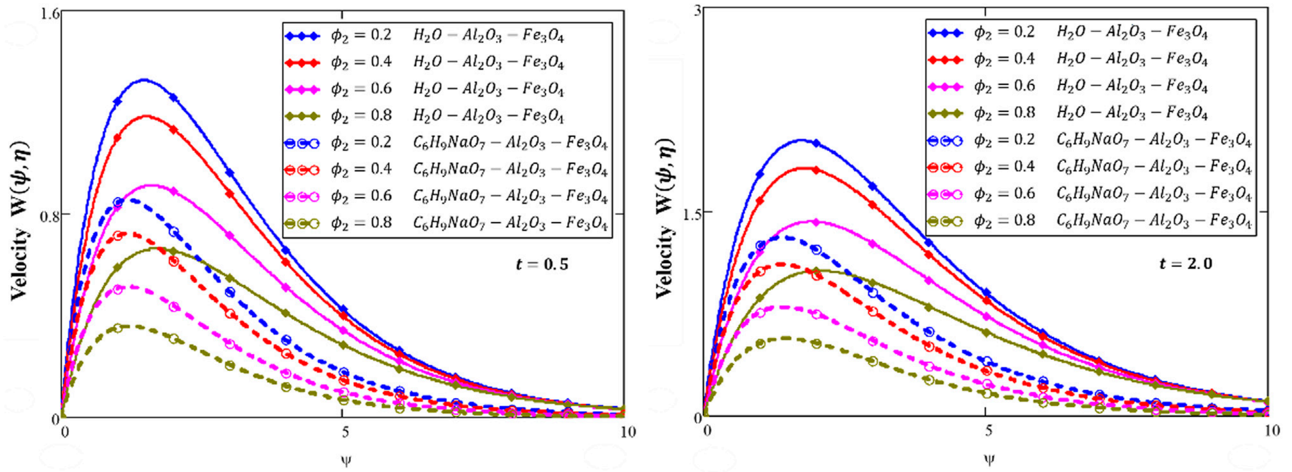

FIGURE 11
Simulation to explain the velocity for fluctuating ϕ_2 when $\alpha = 0.5, Pr = 3.2, \phi_1 = 0.2, Gr = 5, Gm = 6, Sc = 0.2, \lambda_1 = 1.7$, *and* $\lambda_1 = 1.3$.

solution of dimensionless fractional equations of energy, concentration, and momentum is obtained with the Laplace method. To observe from the physical perception, the impacts of fractional derivatives and different flow parameters on concentration, velocity, and temperature are measured and shown in Figures 2–15 graphically.

Figure 2 shows the influence of α on the temperature field. By setting other parameters constant and fluctuating the value of α, it is seen that for a small time, the temperature profile declined for larger values α and this effect is reversed for a greater time. We see that fluid characteristics can be measured by fractional parameters. For a different value of α, the temperature close to the plate is extreme. The temperature declines away from the plate and is asymptotic in the growing ξ direction, which satisfies our boundary conditions. Figure 3 shows the thermal behavior for Pr. For large estimations of Pr, the temperature declines. Substantially, the heat conductivity increasing the estimations of Pr, manufacturing the fluid thicker, sources the least thickness of the heat boundary layer. Figures 4, 5 show the temperature behavior with ϕ_1 and ϕ_2. The temperature field represents an increasing function of ϕ_1 and ϕ_2. As expected, with greater values of ϕ_1 and ϕ_2, the capacity of the HNF expands to hold additional heat. Therefore, the heat conductivity of the NF increases and temperature increases at different times.

The fluid velocity declines as we increase α, as shown in Figure 6, when there is less time. For a long time, the velocity is enhanced. Physically, when α increases, the velocity and thermal boundary layer decline, and as a consequence, the velocity declines for a short time. Figure 7 shows the behavior of the

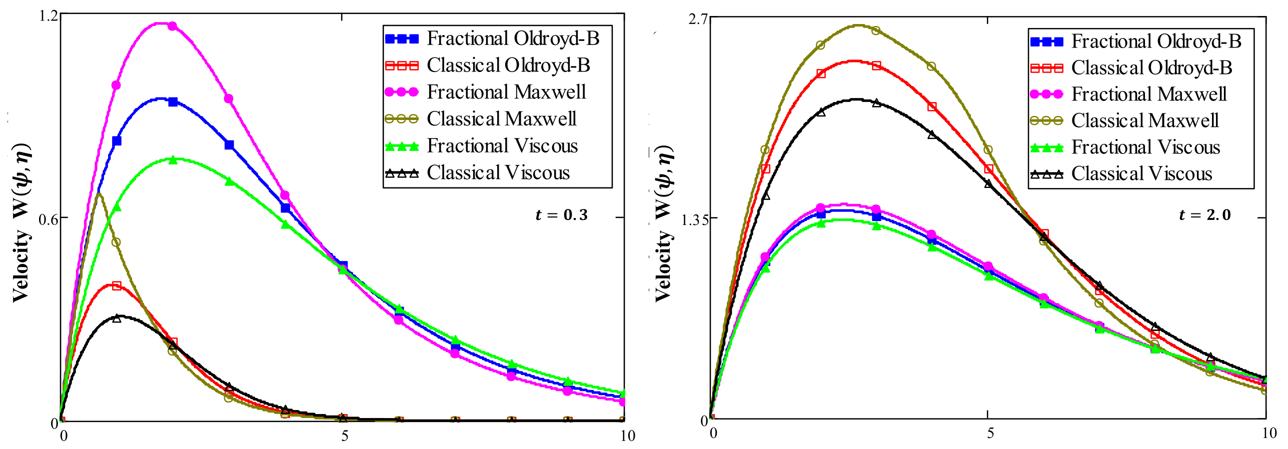

FIGURE 12
Simulation to explain the velocity for the different fluid models when $Pr = 3.2, \phi_1 = \phi_2 = 0.2, Gr = 8, Gm = 4.5, Sc = 0.1, \lambda_1 = 0.7, and\, \lambda_1 = 0.3$.

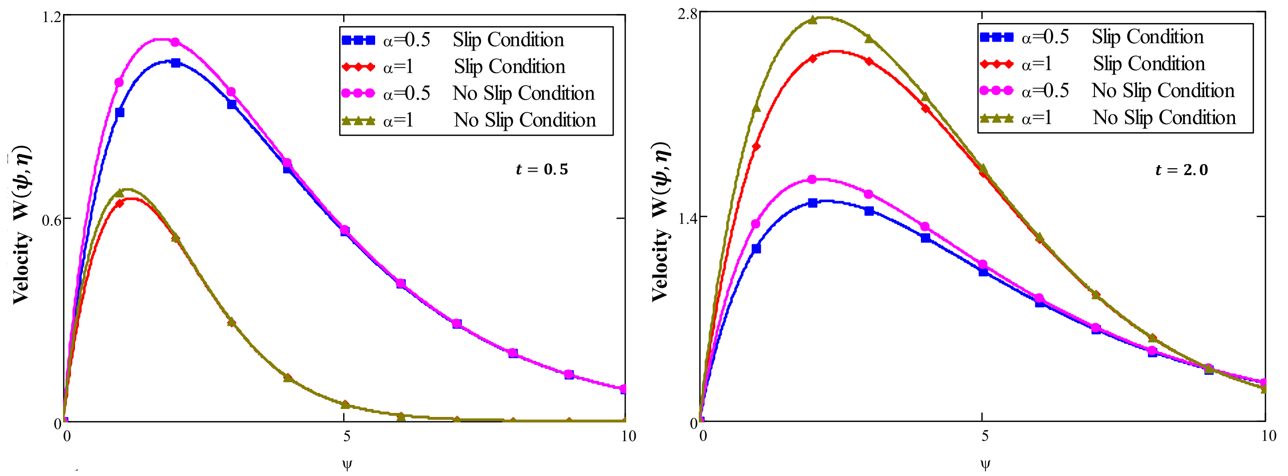

FIGURE 13
Simulation to clarify the velocity for the slip and no-slip condition when $Pr = 6.2, \phi_1 = \phi_2 = 0.2, Gr = 8, Gm = 4.5, Sc = 0.5, \lambda_1 = 0.7, and\, \lambda_1 = 0.3$.

velocity with Pr. The velocity field also decreases with increasing Pr. Enhancement in Pr decreases the thermal conductivity and increases the viscosity of the fluid because of which the momentum profile declines with Pr.

Figure 8 shows the influence of Gr on the momentum profile. By increasing Gr, the velocity profile is enhanced. Since Gr exhibits the buoyancy force that increases the natural convection, therefore the velocity grows. Figure 9 shows the impact of Gm on the velocity by considering the changing Gm with time. The ratio of the buoyant force and viscous force is named the mass Grashof number that sources unrestricted convection. Figure 9 shows that velocity is enhanced for enhancing Gm. Figures 10, 11 show the effect of ϕ_1 and ϕ_2 on velocity. The velocity decreases with increase in ϕ_1 and ϕ_2. This means that with the addition of nanoparticles to the base liquids, the resulting HNF becomes denser, so they become more viscous than the regular fluid. Also, the boundary layer of regular fluids is thinner than that of the HNF, and as a result, the velocity shows a declining behavior with increasing values of ϕ_1 and ϕ_2. Moreover, the impact of a water-based HNF has more progressive values as compared to that of the sodium alginate-based HNF on the profiles of energy and velocity.

Figure 12 shows a comparison of different fluid models. It is observed that the solutions of Maxwell nanofluids for both ordinary and fractional cases have developed curves as compared to Oldroyd-B and viscous nanofluids. Figure 13 shows the velocity for the slip

10.3389/fmats.2023.1114665

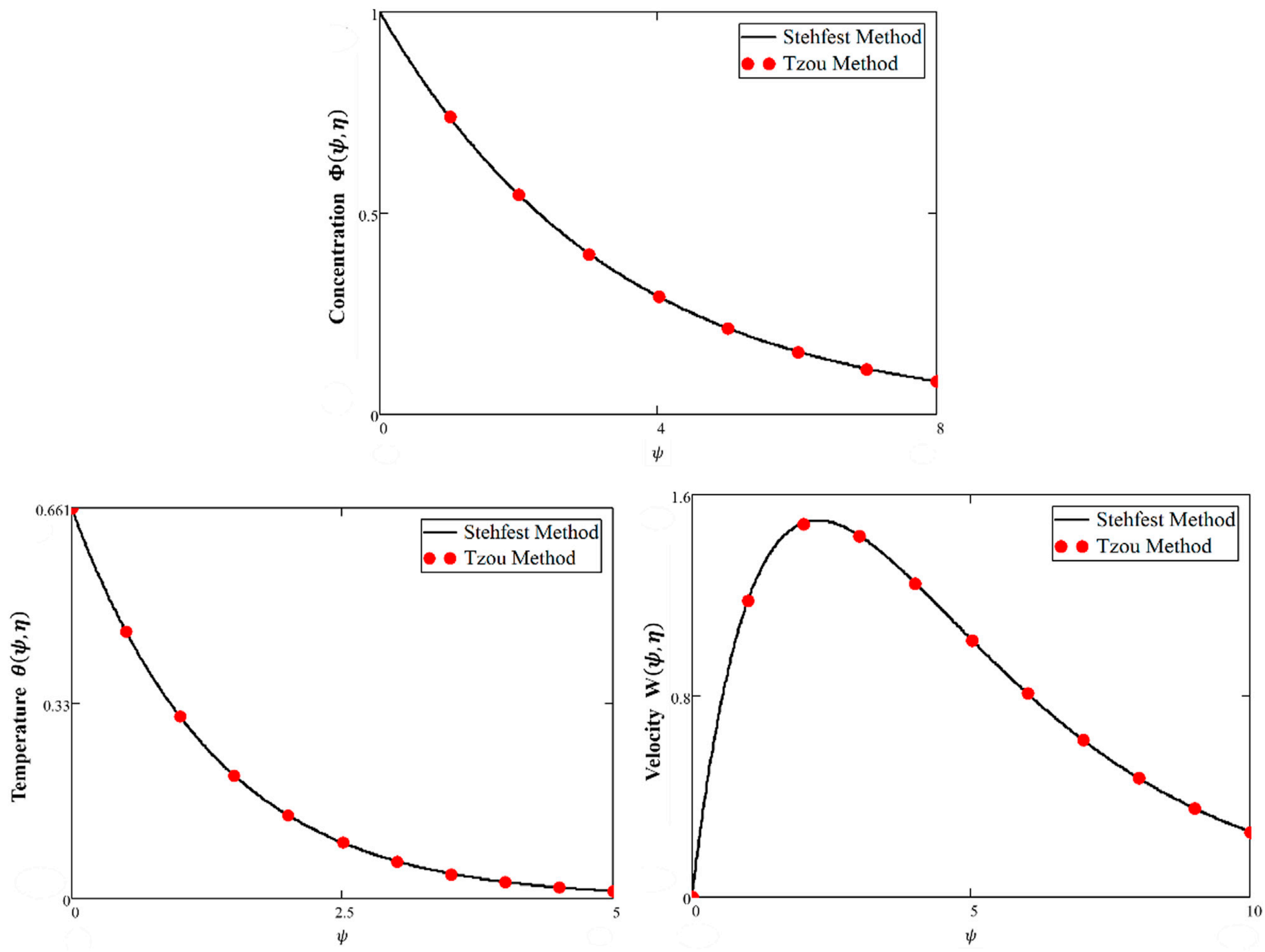

FIGURE 14
Simulation to explain the concentration, temperature, and velocity for the comparison of different inversion numerical algorithms.

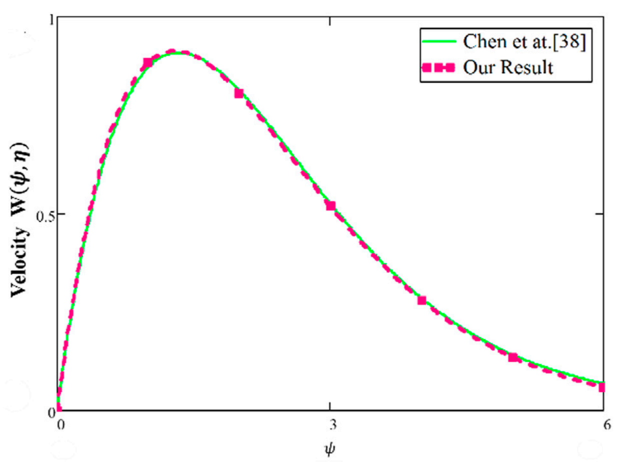

FIGURE 15
Comparison of our results with the results by Chen et al. (2022) for validation.

TABLE 3 Numerical results of the Nusselt number, Sherwood number, and skin friction.

α	t	Pr/Sc	Nu	Sh	C_f
0.3	0.5	5.0	0.3207866	0.45205	1.5162
0.4	0.5	5.0	0.3283006	0.45637	1.4984
0.5	0.5	5.0	0.3381411	0.46149	1.4724
0.5	0.3	5.0	0.214407	0.48954	1.4648
0.5	0.4	5.0	0.2783016	0.47409	1.4651
0.5	0.5	5.0	0.3381411	0.46149	1.4724
0.5	0.5	4.7	0.2101954	0.47599	1.4787
0.5	0.5	4.8	0.2116243	0.471	1.4765
0.5	0.5	4.9	0.2130279	0.46617	1.4744

and no-slip conditions. It can be seen that the slip condition shows a lesser profile for velocity than the no-slip conditions. Figure 14 shows the temperature and velocity behaviors for the comparison of

TABLE 4 Numerical results of comparisons of the velocity field.

ψ	Temperature by our result	Velocity by our result	Temperature by Chen et al. (2022)	Velocity by Chen et al. (2022)	Temperature difference (%)	Velocity difference (%)
0.1	0.2156	0.1693	0.2111	0.1648	2.1317	2.7306
0.6	0.1523	0.7126	0.1475	0.6964	3.2542	2.3262
1.1	0.1069	0.9015	0.1031	0.8917	3.6857	1.099
1.6	0.0747	0.8901	0.0721	0.8913	3.6061	0.1346
2.1	0.0519	0.7805	0.0504	0.7885	2.9762	1.0146
2.6	0.0359	0.6358	0.0352	0.6449	1.9886	1.4111
3.1	0.0247	0.4915	0.0246	0.4986	0.4065	1.424
3.6	0.017	0.365	0.0172	0.3701	1.1628	1.378
4.1	0.0116	0.2624	0.012	0.267	3.3333	1.7228

diverse numerical techniques (Stehfest and Tzou's algorithm). The overlapping of profiles shows that these algorithms are strongly validated with each other. Figure 15 shows the validation of our results with Chen et al. (2022). By overlapping both curves, it is observed from these graphs that our achieved results match those developed by Chen et al. (2022). The numerical comparison of energy, concentration, and velocity profiles by different numerical methods is shown in Table 2. Table 3 shows the numerical results of the Nusselt number, Sherwood number, and skin friction. The comparison of the momentum profile with the work of Chen et al. (2022) is shown in Table 4.

5 Conclusion

This article examines the investigations of the unsteady, convective flow of the Oldroyd-B HNF flowing over a flat plate with wall slip conditions on temperature and constant concentration. The model is developed using the AB-fractional operator and solved with the Laplace transform method. The Laplace inversion is computed with the well-known Stehfest and Tzou numerical schemes. Finally, the effect of diverse flow parameters is planned to estimate the physical clarification of the achieved results of governed equations. The main results from the previous section are summarized in the following:

❖ For a short time, the temperature and momentum profile decayed for a larger value of α, and this effect for both profiles is reversed for a longer time.
❖ By increasing Pr, the temperature and velocity show a decreasing behavior.
❖ By increasing Gm and Gr, the velocity profile is improved.
❖ The velocity decreases with increasing ϕ_1 and ϕ_2.
❖ The energy and velocity profiles are larger for a water-based HNF than those of the sodium alginate-based HNF.
❖ The graphs of Maxwell nanofluids for both classical and fractional models have more advanced curves than Oldroyd-B and viscous nanofluids.
❖ The slip condition shows a lower profile for velocity than the no-slip condition.
❖ The comparison of diverse numerical algorithms (Stehfest and Tzou) strongly validated our study's solutions.
❖ Chen et al. (2022), the overlapping of both curves validate the achieved results of our study.

6 Future recommendation

For extension of this fractional problem examined in this article, we idolized the following proposal based on investigation, approaches, extensions, and geometries, as demarcated in the following:

- The same problem can also be considered over a horizontal plate by using Prabhakar's time-fractional approach with an MHD effect in a porous medium.
- A comparative study of this study can be solved by the natural and Laplace transform methods.
- The same problem may be discussed by the Keller–box scheme.

Data availability statement

The original contributions presented in the study are included in the article/Supplementary Material; further inquiries can be directed to the corresponding author.

Author contributions

Conceptualization, SME, AR, QA, MA, and UK; methodology, SME, AR, and UK; software, MA, QA, SME, AR, and UK; validation, SME, AR, UK, SE, MA, and AhA; formal analysis, AbA, SE, AR, and AhA; investigation, UK, AbA, SE, and AhA; resources, AbA; data curation, QA; writing—original draft preparation, MA, SME, QA, UK, AbA, SE, and AhA; writing—review and editing, AbA, QA, MA, and AhA; visualization, AR, AhA, and SE; supervision, UK; project administration, SE; funding acquisition, SE. All authors have read and agreed to the published version of the manuscript.

Funding

This work received support from Princess Nourah bint Abdulrahman University Researchers Supporting Project number (PNURSP2023R163), Princess Nourah bint Abdulrahman University, Riyadh, Saudi Arabia. In addition, this study is also funded by Prince Sattam bin Abdulaziz University project number (PSAU/2023/R/1444).

Acknowledgments

The authors are thankful for the support of Princess Nourah bint Abdulrahman University Researchers Supporting Project number (PNURSP2023R163), Princess Nourah bint Abdulrahman University, Riyadh, Saudi Arabia. Also, this work is supported *via* funding from Prince Sattam bin Abdulaziz University project number (PSAU/2023/R/1444).

Conflict of interest

The authors declare that the research was conducted in the absence of any commercial or financial relationships that could be construed as a potential conflict of interest.

Publisher's note

All claims expressed in this article are solely those of the authors and do not necessarily represent those of their affiliated organizations, or those of the publisher, the editors, and the reviewers. Any product that may be evaluated in this article, or claim that may be made by its manufacturer, is not guaranteed or endorsed by the publisher.

References

Ahmed, Awais, Alhowaity, Sawsan, and Mohamed, E. (2022). Ghoneim, fehmi gamaoun, elsayed tag-eldin, mansour F. Yassen, and mahnoor sarfraz. "Material and wave relaxation phenomena effects on the rheology of Maxwell nanofluids. *Front. Phys.* 10, 886.

Ali, Qasim, Al-Khaled, Kamel, Ijaz Khan, M., Khan, Sami Ullah, Ali, Raza, Oreijah, Mowffaq, et al. (2022). Diffusion phenomenon for natural convection flow of classical hartmann problem due to a cylindrical tube by generalized fourier's theories: A fractional analysis. *Int. J. Mod. Phys. B* 13, 2350104. doi:10.1142/s0217979223501047

Ali, Qasim, Al-Khaled, Kamel, Omar, Jiyan, Ali, Raza, Khan, Sami Ullah, Ijaz Khan, M., et al. (2022). Analysis for advection–diffusion problem subject to memory effects and local and nonlocal kernels: A fractional operators approach. *Int. J. Mod. Phys. B* 15, 2350099. doi:10.1142/s0217979223500996

Ali, Qasim, Riaz, Samia, Aziz Ullah, Awan, and Ali Abro, Kashif (2021). A mathematical model for thermography on viscous fluid based on damped thermal flux. *Z. für Naturforsch. A* 76 (3), 285–294. doi:10.1515/zna-2020-0322

Asogwa, Kanayo K., Bilal, Sardar M., Animasaun, Isaac L., and Mebarek-Oudina, Fateh M. (2021). Insight into the significance of ramped wall temperature and ramped surface concentration: The case of Casson fluid flow on an inclined Riga plate with heat absorption and chemical reaction. *Nonlinear Eng.* 10 (1), 213–230. doi:10.1515/nleng-2021-0016

Asogwa, Kanayo Kenneth, Goud, B. Shankar, Shah, Nehad Ali, and -Jin Yook, Se (2022). Rheology of electromagnetohydrodynamic tangent hyperbolic nanofluid over a stretching riga surface featuring dufour effect and activation energy. *Sci. Rep.* 12 (1), 14602. doi:10.1038/s41598-022-18998-9

Asogwa, Kanayo Kenneth, Goud, B. Shankar, Yanala Dharmendar Reddyand Ibe, Amarachukwu A. (2022). Suction effect on the dynamics of EMHD casson nanofluid over an induced stagnation point flow of stretchable electromagnetic plate with radiation and chemical reaction. *Results Eng.* 15 (2022), 100518. doi:10.1016/j.rineng.2022.100518

Asogwa, Kanayo Kenneth, Prasad, K. C. Rajendra, Kumar, Raman, Murtugudde, Gururaj, and Punith Gowda, R. J. (2022). Transient electromagnetohydrodynamic Nanofluid flow traveling through a moving Riga plate subject to radiation and heat absorption. *Int. J. Mod. Phys. B* 09, 2350168. doi:10.1142/s0217979223501680

Asogwa, Kanayo K., Mebarek-Oudina, F., and Animasaun, I. L. (2022). Comparative investigation of water-based Al2O3 nanoparticles through water-based CuO nanoparticles over an exponentially accelerated radiative Riga plate surface via heat transport. *Arabian J. Sci. Eng.* 47 (7), 8721–8738. doi:10.1007/s13369-021-06355-3

Atangana, Abdon, and Dumitru, Baleanu (2016). New fractional derivatives with nonlocal and non-singular kernel: Theory and application to heat transfer model. *arXiv Prepr. arXiv:1602.03408* 21.

Awan, Aziz Ullah, Shah, Nehad Ali, Ahmed, Najma, Ali, Qasim, and Riaz, Samia (2019). Analysis of free convection flow of viscous fluid with damped thermal and mass fluxes. *Chin. J. Phys.* 60, 98–106. doi:10.1016/j.cjph.2019.05.006

Batool, Saima, Rasool, Ghulam, Alshammari, Nawa, Khan, Ilyas, Kaneez, Hajra, and Hamadneh, Nawaf (2022). Numerical analysis of heat and mass transfer in micropolar nanofluids flow through lid driven cavity: Finite volume approach. *Case Stud. Therm. Eng.* 37 (2022), 102233. doi:10.1016/j.csite.2022.102233

Chen, C., Rehman, A. U., Riaz, M. B., Jarad, F., and Sun, X.-E. (2022). Impact of Newtonian heating via fourier and Fick's laws on thermal transport of Oldroyd-B fluid by using generalized mittag-leffler kernel. *Symmetry* 14 (4), 766. doi:10.3390/sym14040766

Farooq, U., Afridi, M. I., Qasim, M., and Lu, D. C. (2018). Transpiration and viscous dissipation effects on entropy generation in hybrid nanofluid flow over a nonlinear radially stretching disk. *Entropy* 20 (9), 668. doi:10.3390/e20090668

Goud, B. Shankar, Reddy, Y. Dharmendar, and Kenneth Asogwa, Kanayo (2022). Inspection of chemical reaction and viscous dissipation on MHD convection flow over an infinite vertical plate entrenched in porous medium with Soret effect. *Biomass Convers. Biorefinery* 29, 1–12. doi:10.1007/s13399-022-02886-3

Hassan, Ali, Hussain, Azad, Arshad, Mubashar, Gouadria, Soumaya, Jan, Awrejcewicz, Galal, Ahmed M., et al. (2022). Insight into the significance of viscous dissipation and heat generation/absorption in magneto-hydrodynamic radiative casson fluid flow with first-order chemical reaction. *Front. Phys.* 10, 605. doi:10.3389/fphy.2022.920372

Khan, Dolat, Kenneth Asogwa, Kanayo, Akkurt, Nevzat, Kumam, Poom, Watthayu, Wiboonsak, and Sitthithakerngkiet, Kanokwan (2022). Development of generalized fourier and Fick's law of electro-osmotic MHD flow of sodium alginate based casson nanofluid through inclined microchannel: Exact solution and entropy generation. *Sci. Rep.* 12 (1), 18646. doi:10.1038/s41598-022-21854-5

Khan, Muhammad Naveed, Ahammad, N. Ameer, Ahmad, Shafiq, and Mohamed Abdelghany, Elkotb (2022). Elsayed Tag-eldin, Kamel Guedri, Khaled A. Gepreel, and Mansour F. Yassen. "Thermophysical features of Ellis hybrid nanofluid flow with surface-catalyzed reaction and irreversibility analysis subjected to porous cylindrical surface. *Front. Phys.* 10, 795.

Khan, M. N., Alhowaity, S., Wang, Z., Alqahtani, A. M., Tag-eldin, E., and Yassen, M. F. (2022). Alqahtani, Elsayed Tag-eldin, and Mansour F. Yassen. "Significance of multiple solutions on the dynamics of ethylene glycol conveying gold and copper nanoparticles on a shrinking surface. *Front. Phys.* 10, 928.

Khan, Umar, Ahmed, Naveed, and Khan, Ilyas (2022). Heat transfer evaluation in MgZn6Zr/C8H18 [(Magnesium-Zinc-Zirconium)/Engine oil] with non-linear solar thermal radiations and modified slip boundaries over 3-dimensional convectively heated surface. *Front. Energy Res.* 12, 351.

Lee, S., Choi, S. U.-S, Li, S., and Eastman, J. A (1999). Measuring thermal conductivity of fluids containing oxide nanoparticles 2, 280–289.

Mahian, Omid, Kolsi, Lioua, Amani, Mohammad, Estellé, Patrice, Ahmadi, Goodarz, Kleinstreuer, Clement., et al. (2019). Recent advances in modeling and simulation of nanofluid flows-Part I: Fundamentals and theory. *Phys. Rep.* 790, 1–48. doi:10.1016/j.physrep.2018.11.004

Martyushev, Semen G., and Sheremet, Mikhail A. (2012). Characteristics of Rosseland and P-1 approximations in modeling nonstationary conditions of convection-radiation heat transfer in an enclosure with a local energy source. *J. Eng. Thermophys.* 21 (2), 111–118. doi:10.1134/s1810232812020026

Mohebbi, Rasul, Mehryan, S. A. M., Izadi, Mohsen, and Mahian, Omid (2019). Natural convection of hybrid nanofluids inside a partitioned porous cavity for application in solar power plants. *J. Therm. Analysis Calorim.* 137, 1719–1733. doi:10.1007/s10973-019-08019-9

Rashad, A. M., Chamkha, Ali J., Ismael, Muneer A., and Taha, Salah. (2018). Magnetohydrodynamics natural convection in a triangular cavity filled with a Cu-Al2O3/water hybrid nanofluid with localized heating from below and internal heat generation. *J. Heat Transf.* 140, 7. doi:10.1115/1.4039213, no.

Rasool, Ghulam, Ahammad, N. Ameer, Ali, Mohamed R., Shah, Nehad Ali, Wang, Xinhua, Shafiq, Anum, et al. (2023). Hydrothermal and mass aspects of MHD non-Darcian convective flows of radiating thixotropic nanofluids nearby a horizontal stretchable surface: Passive control strategy. *Case Stud. Therm. Eng.* 42 (2023), 102654. doi:10.1016/j.csite.2022.102654

Rasool, Ghulam, Shafiq, Anum, Hussain, Sajjad, Zaydan, Mostafa, Wakif, Abderrahim, Ali, J., et al. (2022). Significance of rosseland's radiative process on reactive Maxwell nanofluid flows over an isothermally heated stretching sheet in the presence of Darcy–forchheimer and Lorentz forces: Towards a new perspective on buongiorno's model. *Micromachines* 133, 368. doi:10.3390/mi13030368, no.

Rasool, G., Ali Shah, N., El-Zahar, E. R., and Wakif, A. (2022). Numerical investigation of EMHD nanofluid flows over a convectively heated riga pattern positioned horizontally in a Darcy-Forchheimer porous medium: Application of passive control strategy and generalized transfer laws. *Waves Random Complex Media* 17, 1–20.

Raza, A., Almusawa, M. Y., Ali, Q., Haq, A. U., Al-Khaled, K., and Sarris, I. E. (2022). Solution of water and sodium alginate-based casson type hybrid nanofluid with slip and sinusoidal heat conditions: A prabhakar fractional derivative approach. *Symmetry* 1412, 2658. doi:10.3390/sym14122658, no.

Reddy, S. C., Asogwa, K. K., Yassen, M. F., AdnanIqbal, Z., M-Eldin, S., et al. (2022). Dynamics of MHD second-grade nanofluid flow with activation energy across a curved stretching surface. *Front. ENERGY Res.* 10. doi:10.3389/fenrg.2022.1007159

Shahsavar, Amin, Moradi, Mehdi, and Bahiraei, Mehdi (2018). Heat transfer and entropy generation optimization for flow of a non-Newtonian hybrid nanofluid containing coated CNT/Fe3O4 nanoparticles in a concentric annulus. *J. Taiwan Inst. Chem. Eng.* 84, 28–40. doi:10.1016/j.jtice.2017.12.029

Shankar Goud, B., Dharmendar Reddy, Y., and Kenneth Asogwa, Kanayo (2022). Chemical reaction, Soret and Dufour impacts on magnetohydrodynamic heat transfer Casson fluid over an exponentially permeable stretching surface with slip effects. *Int. J. Mod. Phys. B*, 2350124. doi:10.1142/s0217979223501242

Stehfest, Harald. (1970). Algorithm 368: Numerical inversion of Laplace transforms [D5]. *Commun. ACM* 13 (1), 47–49. doi:10.1145/361953.361969

Tzou, Da Yu (2014). *Macro-to microscale heat transfer: The lagging behavior*.Hoboken, NJ, USA John Wiley & Sons.

Usman, M., Hamid, M., Zubair, T., Ul Haq, Rizwan, and Wang, Wei. (2018). Cu-AlO/Water hybrid nanofluid through a permeable surface in the presence of nonlinear radiation and variable thermal conductivity via LSM. *Int. J. Heat Mass Transf.* 126, 1347–1356. doi:10.1016/j.ijheatmasstransfer.2018.06.005

Vallejo, Javier P., Zyla, G., Fernandez-Seara, J., and Lugo, L. (2019). Influence of six carbon-based nanomaterials on the rheological properties of nanofluids. *Nanomaterials* 9 (2), 146. doi:10.3390/nano9020146

Vallejo, J. P., Álvarez-Regueiro, E., Cabaleiro, D., Fernández-Seara, J., Fernández, J., and Lugo, L. (2019). Functionalized graphene nanoplatelet nanofluids based on a commercial industrial antifreeze for the thermal performance enhancement of wind turbines. *Appl. Therm. Eng.* 152, 113–125. doi:10.1016/j.applthermaleng.2019.02.046

Waini, Iskandar, Ishak, Anuar, and Pop, Ioan (2019). Unsteady flow and heat transfer past a stretching/shrinking sheet in a hybrid nanofluid. *Int. J. heat mass Transf.* 136, 288–297. doi:10.1016/j.ijheatmasstransfer.2019.02.101

Wong, Kaufui V., and Omar De, Leon (2010). Applications of nanofluids: Current and future. *Adv. Mech. Eng.* 2, 519659. doi:10.1155/2010/519659

Zhang, Juan, Ali, Raza, Khan, Umair, Ali, Qasim, Zaib, Aurang, Weera, Wajaree, et al. (2022). Thermophysical study of Oldroyd-B hybrid nanofluid with sinusoidal conditions and permeability: A prabhakar fractional approach. *Fractal Fract.* 67, 357. doi:10.3390/fractalfract6070357, no.